Fast Volumetric Registration in MR Images Based on an Accelerated Viscous Fluid Model

Herng-Hua Chang and Yu-Hsuan Chao
Computational Biomedical Engineering Laboratory (CBEL)
Department of Engineering Science and Ocean Engineering
National Taiwan University
Taipei, Taiwan
Email: herbertchang@ntu.edu.tw, r04525065@ntu.edu.tw

***Abstract*—Medical image registration plays an essential role in subsequent image processing and analysis. The demand of direct 3D registration of volumetric image data has been arisen due to the increasing amount of medical image data. This paper investigates a fast volumetric image registration algorithm based on an incompressible viscous fluid model. While direct extension and implementation from 2D fluid registration is inaccessible, we develop numerical techniques to accelerate the computation based on the alternating direction implicit (ADI) scheme. In consequence, the computational complexity is significantly reduced from $O(N^3)$ to $O(N)$. Not only does the computation time expedite, but the memory usage is also cut down. Massive experiments with both simulated and clinical magnetic resonance (MR) image data were administered to qualitatively and quantitatively evaluate the proposed 3D image registration framework. Experimental results suggested that our accelerated image registration algorithm produced high accuracy on both 2D and 3D image registration scenarios and outperformed competing methods. We believe that the proposed volumetric image registration scheme is promising in processing MR image volumes for further medical applications.**

Keywords—volumetric image registration, viscous fluid model, acceleration, alternating direction implicit (ADI), MRI

I. INTRODUCTION

Image registration has been one of the fundamental tasks within medical image processing and analysis. It is the process of determining the correspondence between anatomical structures in two images, which are respectively called the template image and the reference image. Given a reference image and a template image, the goal is to find an appropriate transformation such that the transformed template image becomes similar or even identical to the reference image. In particular, image registration is essential to various magnetic resonance (MR) images in many research and clinical applications such as diagnosis, therapy and surgery planning, and tracking of physical deformations (e.g., tumor growth, brain atrophy) [1, 2].

Recently, there is an increasing need for the direct 3D registration of volumetric images. For example, Lee et al. [3] presented a multiple and simultaneous retinal surface registration method to register surfaces extracted from ocular volumetric optical coherence tomography (OCT) images. The method consisted of using surface currents to enable a point-to-point correspondence between template and subject surfaces. Heyde et al. [4] proposed an anatomical free-form deformation image registration framework using volume conservation to evaluate cardiac deformation from 3D ultrasound images. Zhou and Rivaz [5] developed a nonrigid symmetric registration scheme for accurate alignment of pre- and post-resection volumetric ultrasound images. An outlier detection method was utilized to identify non-corresponding regions, which improved the robustness and accuracy of registration. A rigid registration method [6] for computed tomography (CT) scans in 3D Radon space based on sparse sampling was introduced. Chilla et al. [7] described a deformable registration-based super-resolution reconstruction framework to handle deformable registration as part of super-resolution in 4D MR image volumes.

As can be realized from the literature, different medical applications fertilized the development of diversified registration approaches. Generally speaking, rigid registration methods are based on coordinate changing by affine transform, which can be a prerequisite for nonrigid registration. On the other hand, nonrigid approaches are often employed to handle large scale and complicated deformations, which can be broadly divided into two major categories: physics-based models and function representations [8]. Among the nonrigid methods, fluid registration [9] is of particular importance in MR image analysis as it can be used to localize regions of anatomical change in longitudinal studies and accommodate large deformations while maintaining a diffeomorphism [10]. To achieve accurate registration in MR images, an adaptive image registration algorithm that made use of a closed incompressible viscous fluid model was uniquely developed [11]. This paper investigates a volumetric image registration algorithm based on the extension of [11] for MR image volumes. While direct computation of the extension of the incompressive viscous fluid model in [11] is impractical and unreachable, the proposed framework exploits numerical acceleration techniques to greatly reduce the computation burden. The outcome is an efficient volumetric registration algorithm while maintaining transformation accuracy for feasible applications. The major contributions of the current work are summarized as follows:

1) Extension of 2D partial differential equations (PDEs) in the viscous fluid model to 3D is derived.
2) Numerical technique of alternating direction implicit (ADI) is investigated to accelerate the computation of the viscosity terms.
3) Computational complexity is significantly reduced from $O(N^3)$ to $O(N)$ with N the image voxel number.
4) Memory usage and running time are dramatically shortened due to the acceleration framework.
5) Massive experiments on both simulated images and clinical data in fair comparison with competitive methods are administered.

This work was supported by the Ministry of Science and Technology of Taiwan under Grant MOST 108-2221-E-002-080-MY3.

II. Volumetric Image Registration

A. Navier-Stoke's Equations

The Navier-Stokes equations for a viscous incompressible fluid in 3D for volumetric image registration can be expressed as

$$\frac{\partial \boldsymbol{u}(\boldsymbol{x},t)}{\partial t} + (\boldsymbol{u}(\boldsymbol{x},t)\cdot\nabla)\boldsymbol{u}(\boldsymbol{x},t) = -\boldsymbol{F} + \frac{1}{Re}\Delta\boldsymbol{u}(\boldsymbol{x},t) \quad (1)$$

where $\boldsymbol{u}$ is the divergence-free velocity vector at position $\boldsymbol{x}$ and time t, Re is the Reynolds number, Δ is the Laplace operator, and $\boldsymbol{F}$ is the body force relevant to template and reference images, which will be discussed later. Herein, we assume that the computation is a closed 3D flow in a cubic domain $\Omega = [0, l_x] \times [0, l_y] \times [0, l_z]$, where l_x, l_y, and l_z represent the dimension of the flow domain that corresponds to the image volume under registration. The six surface boundaries of east, west, south, north, top, and bottom are denoted as $\boldsymbol{E}$, $\boldsymbol{W}$, $\boldsymbol{S}$, $\boldsymbol{N}$, $\boldsymbol{T}$, and $\boldsymbol{B}$, each of which is time invariant and nonslip.

In the above equation, the nonlinear term $(\boldsymbol{u}(\boldsymbol{x},t)\cdot\nabla)\boldsymbol{u}(\boldsymbol{x},t)$ originates from the movement of the fluid, which can be resolved in 3D as

$$(\boldsymbol{u}(\boldsymbol{x},t)\cdot\nabla)\boldsymbol{u}(\boldsymbol{x},t) = \left(u\frac{\partial}{\partial x} + v\frac{\partial}{\partial y} + w\frac{\partial}{\partial z}\right)\begin{bmatrix}u\\v\\w\end{bmatrix} = \begin{bmatrix}uu_x + vu_y + wu_z\\ uv_x + vv_y + wv_z\\ uw_x + vw_y + ww_z\end{bmatrix}. \quad (2)$$

Substituting (2) into (1) and decomposing the Navier-Stokes equation into three components, we have

$$u_t + f_x = -(u^2)_x - (uv)_y - (uw)_z + \frac{1}{Re}(u_{xx} + u_{yy} + u_{zz}) \quad (3a)$$

$$v_t + f_y = -(v^2)_y - (uv)_x - (vw)_z + \frac{1}{Re}(v_{xx} + v_{yy} + v_{zz}) \quad (3b)$$

$$w_t + f_z = -(w^2)_z - (uw)_x - (vw)_y + \frac{1}{Re}(w_{xx} + w_{yy} + w_{zz}) \quad (3c)$$

where $\boldsymbol{u} = (u, v, w)$ and f_x, f_y, and f_z represent the body force $\boldsymbol{F}$ in the x-, y-, and z-axis, respectively. In the above equations, the first terms on the right hand side are the inertia or called the convection term, and the last terms are the diffusion or called the viscosity term.

B. Convection Term Computation

We first assume that the continuity condition div $\boldsymbol{u} = 0$ is satisfied and the velocity fields u^n, v^n, and w^n at the n^{th} time step are known. A splitting strategy is introduced to avoid direct computation of the nonlinear terms by incorporating a vector of intermediate velocity (u^*, v^*, w^*) corresponding to $\boldsymbol{u}^n$ into the convection terms using

$$\begin{aligned}\frac{u^*-u^n}{\Delta t} &= -((u^n)^2)_x - (u^n v^n)_y - (u^n w^n)_z\\ \frac{v^*-v^n}{\Delta t} &= -((v^n)^2)_y - (u^n v^n)_x - (v^n w^n)_z\\ \frac{w^*-w^n}{\Delta t} &= -((w^n)^2)_z - (u^n w^n)_x - (v^n w^n)_y\end{aligned} \quad (4)$$

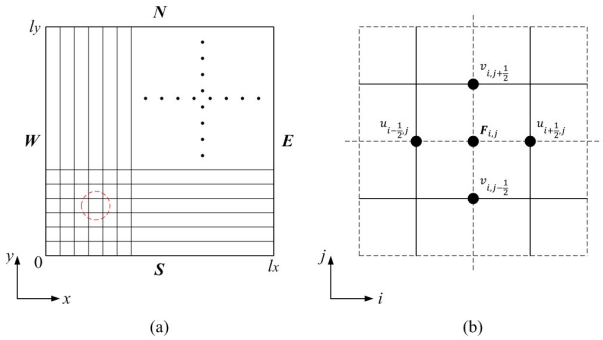

Fig. 1. (a) Illustration of the 3D flow in the $\boldsymbol{xy}$ plane and boundary symbols. This flow domain corresponds to one slice of the image volume under registration. (b) Illustration of staggered grids for the triple $\boldsymbol{F}$, $\boldsymbol{u}$ and $\boldsymbol{v}$ in a grid cell with respect to the arbitrarily circled voxel in (a).

where Δt is the time step. To prevent unstable problems, it is needed to satisfy the Courant-Friedrich-Levy (CFL) condition.

Since the staggered grid scheme is adopted, direct computation of the velocity terms in (4) at the same grid point is inaccessible. To solve (4), say, updating u, we define u^2 at the cell center and uv (or uw) at the cell corners as illustrated in Fig.1 and formulated as

$$(u^2)_{i+\frac{1}{2},j,k} = \left(\frac{u_{i,j,k}+u_{i+1,j,k}}{2}\right)^2 \quad (5a)$$

$$u_{i,j+\frac{1}{2},k}v_{i+\frac{1}{2},j,k} = \left(\frac{u_{i,j,k}+u_{i,j+1,k}}{2}\right)\left(\frac{v_{i,j,k}+v_{i+1,j,k}}{2}\right) \quad (5b)$$

$$u_{i,j,k+\frac{1}{2}}w_{i+\frac{1}{2},j,k} = \left(\frac{u_{i,j,k}+u_{i,j,k+1}}{2}\right)\left(\frac{w_{i,j,k}+w_{i+1,j,k}}{2}\right). \quad (5c)$$

Similarly, the velocity computation for v and w can be respectively expressed as

$$(v^2)_{i,j+\frac{1}{2},k} = \left(\frac{v_{i,j,k}+v_{i,j+1,k}}{2}\right)^2 \quad (6a)$$

$$u_{i,j+\frac{1}{2},k}v_{i+\frac{1}{2},j,k} = \left(\frac{u_{i,j,k}+u_{i,j+1,k}}{2}\right)\left(\frac{v_{i,j,k}+v_{i+1,j,k}}{2}\right) \quad (6b)$$

$$v_{i,j,k+\frac{1}{2}}w_{i,j+\frac{1}{2},k} = \left(\frac{v_{i,j,k}+v_{i,j,k+1}}{2}\right)\left(\frac{w_{i,j,k}+w_{i,j+1,k}}{2}\right) \quad (6c)$$

and

$$(w^2)_{i,j,k+\frac{1}{2}} = \left(\frac{w_{i,j,k}+w_{i,j,k+1}}{2}\right)^2 \quad (7a)$$

$$u_{i,j,k+\frac{1}{2}}w_{i+\frac{1}{2},j,k} = \left(\frac{u_{i,j,k}+u_{i,j,k+1}}{2}\right)\left(\frac{w_{i,j,k}+w_{i+1,j,k}}{2}\right) \quad (7b)$$

$$v_{i,j,k+\frac{1}{2}}w_{i,j+\frac{1}{2},k} = \left(\frac{v_{i,j,k}+v_{i,j,k+1}}{2}\right)\left(\frac{v_{i,j,k}+v_{i,j+1,k}}{2}\right). \quad (7c)$$

Apparently, the above velocity computation is based on the average of two grid points and we can rewrite (4) as

$$\begin{aligned}\frac{u^*-u^n}{\Delta t} &= -((\bar{u}^h)^2)_x - (\bar{u}^v\bar{v}^h)_y - (\bar{u}^t\bar{w}^h)_z\\ \frac{v^*-v^n}{\Delta t} &= -((\bar{v}^v)^2)_y - (\bar{u}^v\bar{v}^h)_x - (\bar{v}^t\bar{w}^v)_z\\ \frac{w^*-w^n}{\Delta t} &= -((\bar{w}^t)^2)_z - (\bar{u}^t\bar{w}^h)_x - (\bar{v}^t\bar{w}^v)_y\end{aligned} \quad (8)$$

where an overbar with superscript h represents a horizontally averaged quantity corresponding to the x-axis, an overbar with superscript v represents a vertically averaged quantity corresponding to the y-axis, and an overbar with superscript t represents an averaged quantity in the thickness direction.

C. Viscosity Term Computation

While the convection terms are computed explicitly, the viscosity terms are treated implicitly to avoid the limitation of spatial discretization using

$$\begin{aligned}\frac{u^{**}-u^{*}}{\Delta t} &= \frac{1}{\mathrm{Re}}\left(u^{**}_{xx}+u^{**}_{yy}+u^{**}_{zz}\right)\\ \frac{v^{**}-v^{*}}{\Delta t} &= \frac{1}{\mathrm{Re}}\left(v^{**}_{xx}+v^{**}_{yy}+v^{**}_{zz}\right)\\ \frac{w^{**}-w^{*}}{\Delta t} &= \frac{1}{\mathrm{Re}}\left(w^{**}_{xx}+w^{**}_{yy}+w^{**}_{zz}\right)\end{aligned} \tag{9}$$

where Δt is the time interval, u^{**}, v^{**}, and w^{**} represents another set of intermediate velocity. Rearranging (9), we can obtain

$$\begin{aligned}u^{*} &= u^{**}-\frac{\Delta t}{\mathrm{Re}}\left(u^{**}_{xx}+u^{**}_{yy}+u^{**}_{zz}\right)\\ v^{*} &= v^{**}-\frac{\Delta t}{\mathrm{Re}}\left(v^{**}_{xx}+v^{**}_{yy}+v^{**}_{zz}\right)\\ w^{*} &= w^{**}-\frac{\Delta t}{\mathrm{Re}}\left(w^{**}_{xx}+w^{**}_{yy}+w^{**}_{zz}\right)\end{aligned} \quad . \tag{10}$$

Considering the computation of u in (10) and expanding the right hand side in the matrix form, we have

$$\begin{bmatrix}1&0&0&\cdots\\0&1&0&\cdots\\0&0&1&\cdots\\\vdots&\vdots&\vdots&\ddots\end{bmatrix}-\frac{\Delta t}{\mathrm{Re}}\left\{\begin{bmatrix}-2&1&0&\cdots\\1&-2&1&\cdots\\0&1&-2&\cdots\\\vdots&\vdots&\vdots&\ddots\end{bmatrix}\frac{1}{(\Delta x)^2}+\begin{bmatrix}-2&0&1&\cdots\\0&-2&0&1\\0&0&-2&\cdots\\\vdots&\vdots&\vdots&\ddots\end{bmatrix}\frac{1}{(\Delta y)^2}+\begin{bmatrix}-2&0&1&\cdots\\0&-2&0&1\\0&0&-2&\cdots\\\vdots&\vdots&\vdots&\ddots\end{bmatrix}\frac{1}{(\Delta z)^2}\right\} \tag{11}$$

where Δx, Δy, and Δz represent the grid spacing in the x-, y-, and z-axis, respectively. In (11), the dimension of each matrix is approximately $N \times N$ with N the image voxel number. To compute u at each voxel requires solving N^2 linear equations, whose computational complexity reaches $O(N^3)$ using the Cholesky decomposition algorithm.

D. Alternating Direction Implicit

We observe the similarity between the second derivative terms on the right hand side in (9) and the heat equation. An approximate solution to (9) can be achieved by using the alternating direction implicit (ADI) algorithm [12]. The proposed strategy requires three major steps in each velocity direction, say, for u, which are

$$\left(1-\frac{r_x}{2}\delta_x^2\right)\Delta u^{*}_{i,j,k} = \left(r_x\delta_x^2+r_y\delta_y^2+r_z\delta_z^2\right)u^{*}_{i,j,k} \tag{12a}$$

$$\left(1-\frac{r_y}{2}\delta_y^2\right)\Delta u^{**}_{i,j,k} = \Delta u^{*}_{i,j,k} \tag{12b}$$

$$\left(1-\frac{r_z}{2}\delta_z^2\right)\Delta u_{i,j,k} = \Delta u^{**}_{i,j,k}. \tag{12c}$$

Similarly, the ADI formulas for approximating v and w are respectively expressed as

$$\left(1-\frac{r_x}{2}\delta_x^2\right)\Delta v^{*}_{i,j,k} = \left(r_x\delta_x^2+r_y\delta_y^2+r_z\delta_z^2\right)v^{*}_{i,j,k} \tag{13a}$$

$$\left(1-\frac{r_y}{2}\delta_y^2\right)\Delta v^{**}_{i,j,k} = \Delta v^{*}_{i,j,k} \tag{13b}$$

$$\left(1-\frac{r_z}{2}\delta_z^2\right)\Delta v_{i,j,k} = \Delta v^{**}_{i,j,k} \tag{13c}$$

and

$$\left(1-\frac{r_x}{2}\delta_x^2\right)\Delta w^{*}_{i,j,k} = \left(r_x\delta_x^2+r_y\delta_y^2+r_z\delta_z^2\right)w^{*}_{i,j,k} \tag{14a}$$

$$\left(1-\frac{r_y}{2}\delta_y^2\right)\Delta w^{**}_{i,j,k} = \Delta w^{*}_{i,j,k} \tag{14b}$$

$$\left(1-\frac{r_z}{2}\delta_z^2\right)\Delta w_{i,j,k} = \Delta w^{**}_{i,j,k}. \tag{14c}$$

In the above equations, the symbols are defined as follows:

$$r_x = \alpha\frac{\Delta t}{(\Delta x)^2} \tag{15a}$$

$$r_y = \alpha\frac{\Delta t}{(\Delta y)^2} \tag{15b}$$

$$r_z = \alpha\frac{\Delta t}{(\Delta z)^2} \tag{15c}$$

where $\alpha = 1/\mathrm{Re}$ and δ_x^2, δ_y^2, and δ_z^2 are the central difference operators.

The ADI equation set in each velocity direction can be further decomposed into a tridiagonal matrix system, whose form are described as

$$\begin{bmatrix}d_1&a_1&0&\cdots&\cdots&\cdots&0\\b_2&d_2&a_2&0&&&\vdots\\0&b_3&d_3&a_3&0&&\vdots\\\vdots&&\ddots&\ddots&\ddots&&\vdots\\\vdots&&&\ddots&\ddots&\ddots&0\\\vdots&&&&\ddots&\ddots&a_{N-1}\\0&\cdots&\cdots&\cdots&0&b_N&d_N\end{bmatrix}\begin{bmatrix}u_1^{n+1}\\u_2^{n+1}\\\vdots\\\vdots\\\vdots\\\vdots\\u_N^{n+1}\end{bmatrix}=\begin{bmatrix}c_1\\c_2\\\vdots\\\vdots\\\vdots\\\vdots\\c_N\end{bmatrix} \tag{16}$$

where a_i, b_i, c_i, and d_i are known corresponding to the unknown variable u_i^{n+1}, which can be one of the three velocity components. The unknown in (16) is rapidly computed using the Thomas scheme associated with the Gauss elimination method, whose computational complexity is simply $O(N)$.

E. Body Force Computation

After obtaining the velocity at the $(n+1)^{th}$ time step, we can relate the intermediate velocity with the body force using

$$\frac{u^{n+1}-u^{**}}{\Delta t} = -f_x^n \tag{17a}$$

$$\frac{v^{n+1}-v^{**}}{\Delta t} = -f_y^n \tag{17b}$$

$$\frac{w^{n+1}-w^{**}}{\Delta t} = -f_z^n \tag{17c}$$

where the body force is defined as

$$\boldsymbol{F} = (T(\boldsymbol{x}-\boldsymbol{d})-R(\boldsymbol{x}))\nabla T(\boldsymbol{x}-\boldsymbol{d}) \tag{18}$$

where T represents the template image, R represents the reference image, $T(\boldsymbol{x}-\boldsymbol{d})-R(\boldsymbol{x})$ is the intensity difference between T and R, $\nabla T(\boldsymbol{x}-\boldsymbol{d})$ gives the direction of the body force, and $\boldsymbol{d} = (d_x, d_y, d_z)$ is the deformation with

$$\boldsymbol{d} = \int \boldsymbol{u}(\boldsymbol{x},t)\mathrm{d}t \tag{19}$$

which is numerically computed using

$$d_x^{n+1} = \tilde{u}^{n+1}\Delta t \tag{20a}$$

$$d_y^{n+1} = \tilde{v}^{n+1}\Delta t \tag{20b}$$

$$d_z^{n+1} = \tilde{w}^{n+1}\Delta t \tag{20c}$$

where $\tilde{u}$, $\tilde{v}$, and $\tilde{w}$ are the smoothed velocity of u, v, and w, respectively. The smoothing process is mainly for reducing the velocity variation due to the noise in the MR image volume, which is executed using a 3D Gaussian filter with a dimension of $(2H+1)\times(2H+1)\times(2H+1)$ with H an integer.

III. Experimental Results

A. Evaluation Metrics

To understand the proposed volumetric image registration algorithm, a variety of both simulated and clinical images acquired from the simulated brain database (SBD) [13] were adopted. To analyze the performance of the proposed image registration scheme, the correlation coefficient (CC) and the sum of squared difference (SSD) before and after registration between the template and reference images were computed as given in the following:

$$\mathrm{CC} = \frac{\sum\sum\sum(A(x,y,z)-\bar{A}(x,y,z))\sum\sum\sum(B(x,y,z)-\bar{B}(x,y,z))}{\sqrt{\sum\sum\sum(A(x,y,z)-\bar{A}(x,y,z))^2\sum\sum\sum(B(x,y,z)-\bar{B}(x,y,z))^2}} \quad (21)$$

and

$$\mathrm{SSD} = \sum\sum\sum\frac{\|A(x,y,z)-B(x,y,z)\|^2}{S} \quad (22)$$

where $\|\cdot\|$ represents the Euclidean norm, S represents the total voxel number, $A(x,y,z)$ and $B(x,y,z)$ represent the intensities of image volumes A and B at (x,y,z), and $\bar{A}$ and $\bar{B}$ represent the average intensities of images A and B, respectively. The higher the CC value and the lower the SSD value, the better the registration performance. The entire system was implemented and programmed in MATLAB 2016 (The MathWorks Inc. Natick, MA, USA). All experiments were executed on an Intel® Core(TM) i5 CPU @ 3.20GHz with 8 GB RAM running 64-bit Windows 7.

B. Registration of 2D Images

Registration of 2D MR images was first executed for interpreting the characteristics the proposed image registration algorithm. Fig. 2 depicts the registration of a 256×256 knee MR image of the proposed framework in comparison to the former fluid registration method [11]. It was hard to visually distinguish between Figs. 2(b), 2(c), and 2(d). Another representative example of registering a 256×256 T1-weighted brain MR image with large deformation is shown in Fig. 3, where close registration results were found again. Table I summarizes the performance evaluation scores and computation time in Figs. 2 and 3. It was noted that the evaluation scores of both methods were comparable whereas the computation time of the proposed algorithm was much less than the classical method [11]. Massive experiments of registration on 96 images with different deformation scenarios further demonstrated the efficacy and accuracy of the proposed acceleration version of fluid registration as presented in Table II.

Experiments on 181×217 T2-weighted brain MR images with extensive distortion were also performed and illustrated in Fig. 4, where a reference image followed by three different template images denoted as t1, t2, and t3 in order are shown in the first row. For comparison, the registration results by Bro-Nielsen and Gramkow [14] are shown in the second row, where the first image indicates the difference image between the registered t1 image and the reference image. As the template images were extremely distorted, it was not easy to transform back to the reference image. In contrast, our registration framework performed better so that the gyrus was closer to the reference image, especially for the ventricle structures as depicted in the last row. Table III reports the evaluation scores of both methods for the experiments in Fig. 4. Not only did the proposed scheme produce better values, but it also spent much less time to complete the task.

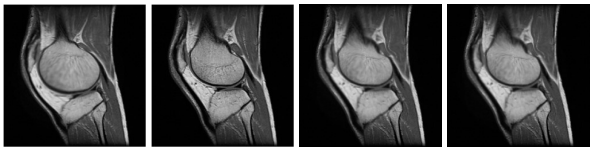

(a) (b) (c) (d)

Fig. 2. Registration of 256×256 knee MR images. (a) Template image. (b) Reference image. (c) Literature [11]. (d) Proposed.

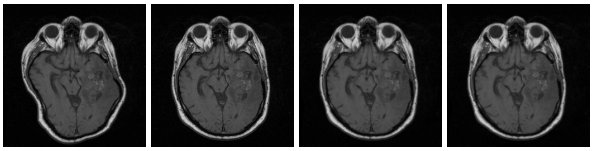

(a) (b) (c) (d)

Fig. 3. Registration of 256×256 T1-weighted brain MR images. (a) Template image. (b) Reference image. (c) Literature [11]. (d) Proposed.

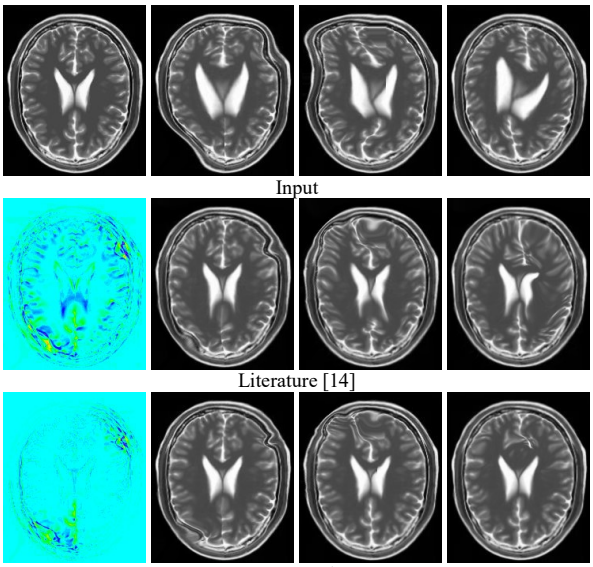

Fig. 4. Registration of 181×217 T2-weighted brain MR images. First row: reference image followed by three template images (t1, t2, and t3). Second row: difference image of t1 followed by the registration of the corresponding template images using the method in literature [14]. Last row: difference image of t1 followed by the registration of the corresponding template images using the proposed algorithm.

TABLE I. PERFORMANCE COMPARISON OF 2D IMAGE REGISTRATION RESULTS.

Image	Evaluation	Before Registration	Literature [11]	Proposed
Fig. 2	CC	0.8449	0.9928	0.9927
	SSD	3.865e-03	1.359e-08	5.944e-08
	Time (s)		193.43	123.70
Fig. 3	CC	0.7529	0.9938	0.9935
	SSD	4.529e-08	4.238e-10	4.401e-10
	Time (s)		1546.42	109.31

TABLE II. PERFORMANCE EVALUATION OF MASSIVE REGISTRATION ON 96 IMAGES.

Metric	Before Registration	Literature [11]	Proposed
CC	0.832±0.175	0.993±0.013	0.993±0.013
SSD	2.91e-08±3.08e-08	7.47e-10±1.71e-09	7.45e-10±1.71e-09

C. Registration of Image Volumes

In Fig. 5, we demonstrate the volumetric image registration outcome of a sphere to an ellipsoid in a $200 \times 200 \times 200$ domain. The challenge of this registration task was mainly due to the extreme deformation in 3D in such a way that shrinking encountered in the xy plane while stretching arisen in the vertical direction. Although few domes at the top and bottom of the registered ellipsoid were missing, it was generally pleasant considering intense geometric difference being confronted. Fig. 6 shows the volumetric image registration results of $192 \times 256 \times 144$ brain MR image volumes. It was clear that the template image volume in Fig. 6(a) was highly distorted in the vertical direction comparing to the reference image volume in Fig. 6(b), which exhibited a quite normal brain dimension ratio. After applying our 3D image registration algorithm, the distorted brain image volume was well registered as illustrated in Fig. 6(c). In Table IV, we summarize the performance evaluation scores of volumetric image registration results in Figs. 5 and 6. It was noted that the CC values were pretty high and the SSD values were tiny in both volumetric image registration scenarios.

IV. Conclusion

We have introduced a new volumetric image registration framework based on an incompressible viscous fluid model. While direct extension and implementation from 2D fluid registration was inaccessible, we developed numerical techniques to accelerate the computation of complex PDEs. The most challenging computation of the viscosity terms was simplified with computational complexity $O(N^3)$ reduced to $O(N)$ based on the ADI scheme. The proposed volumetric image registration algorithm was validated on massive experiments with both simulated and clinical MR image data. Experimental results suggested that our accelerated image registration framework produced high accuracy on both 2D and 3D image registration scenarios and outperformed competing methods. It is believed that the proposed volumetric image registration algorithm is promising in handling clinical MR image volumes for further medical image processing applications.

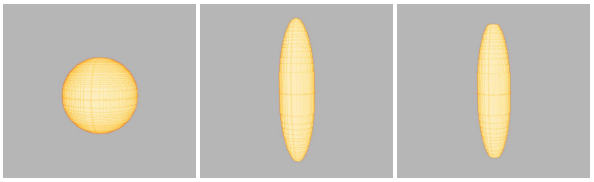

(a) (b) (c)

Fig. 5. Registration of $200 \times 200 \times 200$ simulated image volumes. (a) Template sphere image volume. (b) Reference ellipsoid image volume. (c) Registration outcome.

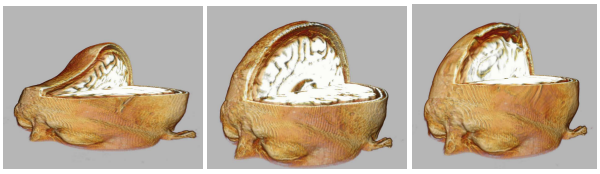

(a) (b) (c)

Fig. 6. Registration of $192 \times 256 \times 144$ brain MR image volumes. (a) Template image volume. (b) Reference image volume. (c) Registration outcome.

TABLE III. PERFORMANCE COMPARISON OF THE BRAIN IMAGE REGISTRATION RESULTS IN FIG. 4.

Image	Evaluation	Before Registration	Literature [14]	Proposed
t1	CC	0.7432	0.9435	0.9755
	SSD	2.06e-07	2.42e-08	8.86e-08
	Time (s)		137.41	40.34
t2	CC	0.7306	0.9332	0.9763
	SSD	2.11e-07	2.95e-08	1.42e-08
	Time (s)		202.12	63.86
t3	CC	0.7891	0.9364	0.9768
	SSD	1.91e-07	3.11e-08	1.40e-08
	Time (s)		241.55	62.31

TABLE IV. PERFORMANCE EVALUATION OF VOLUMETRIC IMAGE REGISTRATION RESULTS.

Image	Evaluation	Before Registration	Proposed
Fig. 5	CC	0.4346	0.9979
	SSD	6.74e-09	1.59e-11
	Time (s)		2905.98
Fig. 6	CC	0.8496	0.9820
	SSD	6.71e-09	8.03e-10
	Time (s)		17736.39

References

[1] J. Villalon, A. A. Joshi, N. Lepore, C. Brun, A. W. Toga, and P. M. Thompson, "Comparison of volumetric registration algorithms for tensor-based morphometry," in *2011 IEEE International Symposium on Biomedical Imaging: From Nano to Macro*, 2011, pp. 1536-1541.

[2] A. Szmul, B. W. Papież, A. Hallack, V. Grau, and J. A. Schnabel, "Supervoxels for graph cuts-based deformable image registration using guided image filtering," 2017, vol. 26, p. 13: SPIE.

[3] S. Lee, E. Lebed, M. V. Sarunic, and M. F. Beg, "Exact Surface Registration of Retinal Surfaces From 3-D Optical Coherence Tomography Images," *IEEE Transactions on Biomedical Engineering,* vol. 62, no. 2, pp. 609-617, 2015.

[4] B. Heyde, M. Alessandrini, J. Hermans, D. Barbosa, P. Claus, and J. D. hooge, "Anatomical Image Registration Using Volume Conservation to Assess Cardiac Deformation From 3D Ultrasound Recordings," *IEEE Transactions on Medical Imaging,* vol. 35, no. 2, pp. 501-511, 2016.

[5] H. Zhou and H. Rivaz, "Registration of Pre- and Postresection Ultrasound Volumes With Noncorresponding Regions in Neurosurgery," *IEEE Journal of Biomedical and Health Informatics,* vol. 20, no. 5, pp. 1240-1249, 2016.

[6] G. Medan, N. Shamul, and L. Joskowicz, "Sparse 3D Radon Space Rigid Registration of CT Scans: Method and Validation Study," *IEEE Transactions on Medical Imaging,* vol. 36, no. 2, pp. 497-506, 2017.

[7] G. S. V. N. Chilla, C. H. Tan, and C. L. Poh, "Deformable Registration-Based Super-resolution for Isotropic Reconstruction of 4-D MRI Volumes," *IEEE Journal of Biomedical and Health Informatics,* vol. 21, no. 6, pp. 1617-1624, 2017.

[8] M. Holden, "A Review of Geometric Transformations for Nonrigid Body Registration," *Medical Imaging, IEEE Transactions on,* vol. 27, no. 1, pp. 111-128, 2008.

[9] G. E. Christensen, R. D. Rabbitt, and M. I. Miller, "Deformable templates using large deformation kinematics," *IEEE Transans on Image Processing,* vol. 5, no. 10, pp. 1435-1447, 1996.

[10] L. A. van de Pol *et al.*, "Improved reliability of hippocampal atrophy rate measurement in mild cognitive impairment using fluid registration," *NeuroImage,* vol. 34, no. 3, pp. 1036-1041, 2007.

[11] H.-H. Chang and C.-Y. Tsai, "Adaptive registration of magnetic resonance images based on a viscous fluid model," *Computer Methods and Programs in Biomedicine,* vol. 117, no. 2, pp. 80-91, 2014/11/01/ 2014.

[12] J. Jim Douglas and J. E. Gunn, "A general formulation of alternating direction methods," *Numer. Math.,* vol. 6, no. 1, pp. 428-453, 1964.

[13] McGill University, *BrainWeb: Simulated Brain Database*. http://www.bic.mni.mcgill.ca/brainweb/, 2016.

[14] M. Bro-Nielsen and C. Gramkow, "Fast Fluid Registration of medical images," in *Visualization in Biomedical Computing: 4th International Conference, VBC'96 Hamburg, Germamy, September 22–25, 1996 Proceedings*, K. H. Höhne and R. Kikinis, Eds. Berlin, Heidelberg: Springer Berlin Heidelberg, 1996, pp. 265-276.